Supplement of "Dense water formation in the North–Central Aegean Sea during winter 2021–2022"

M. Potiris[1], I. Mamoutos[1], E. Tragou[1], V. Zervakis[1], D. Kassis[2], and D. Ballas[2]

[1]*Department of Marine Sciences, School of the Environment, University of the Aegean, Mytilene, Lesvos, 81132, Greece*

[2]*Institute of Oceanography, Hellenic Centre for Marine Research, Anavyssos, Attica, 19013, Greece*

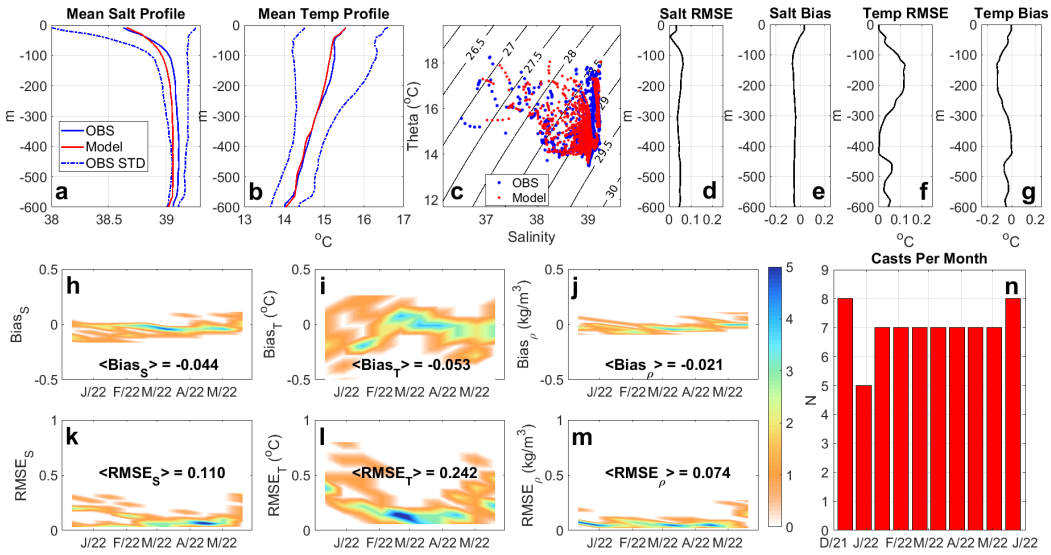

Figure S1: Time-mean and standard deviation of (a) salinity and (b) temperature profiles from Argo observations compared to the time-mean model profiles. (c) Model and observations θ/S diagram. Salinity (d) root mean square error and (e) bias profiles between model output and Argo observations. Temperature (f) root mean square error and (g) bias profiles between model output and Argo observations. Time-dependent correlation, bias and root mean square error for (h, k) salinity, (j, l) temperature, and (j, m) density, between model output and observations. (n) Number of profile observations per month.

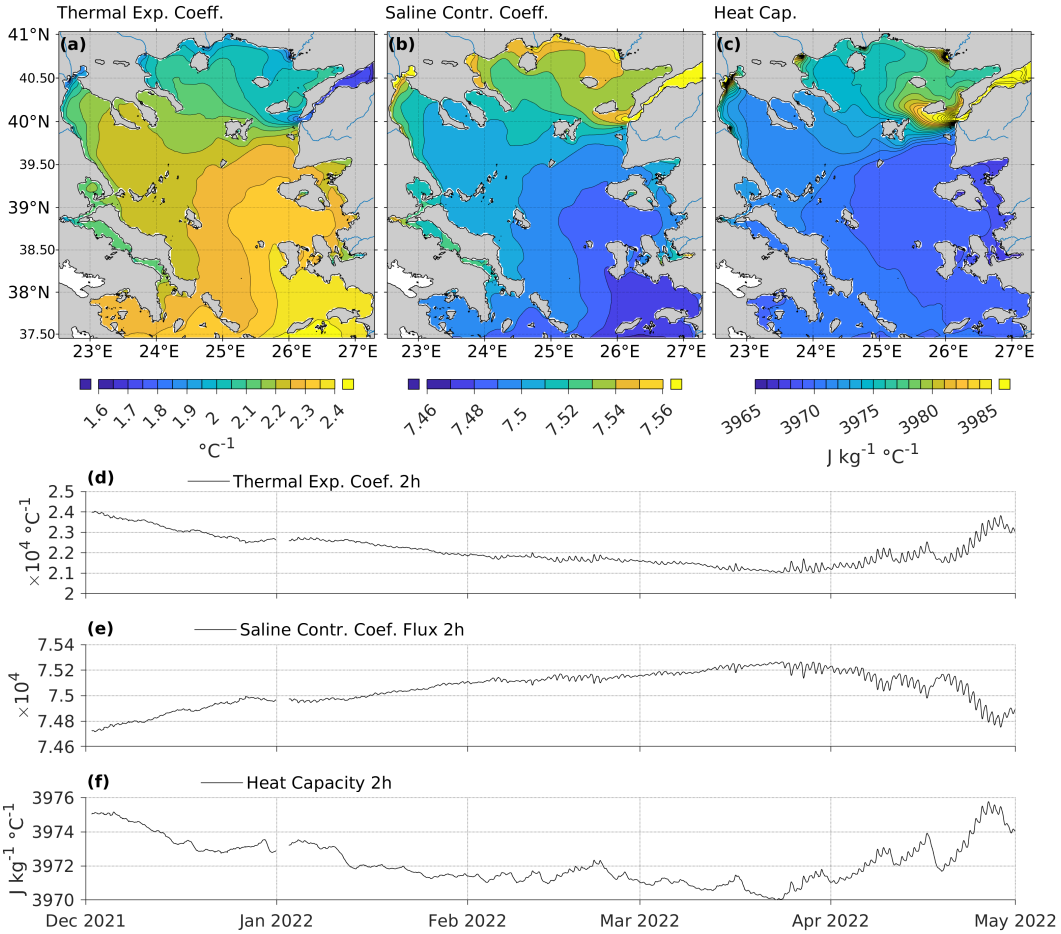

Figure S2: Spatiotemporal variability of thermodynamic properties of sea water from 2 December 2021 –30 April 2022 over the study area. Time-mean (a) thermal expansion coefficient a, (b) saline contrac-tion coefficient b, and (c) heat capacity C_p. Field-mean (d) thermal expansion coefficient a, (e) saline contraction coefficient b, and (f) heat capacity C_p.

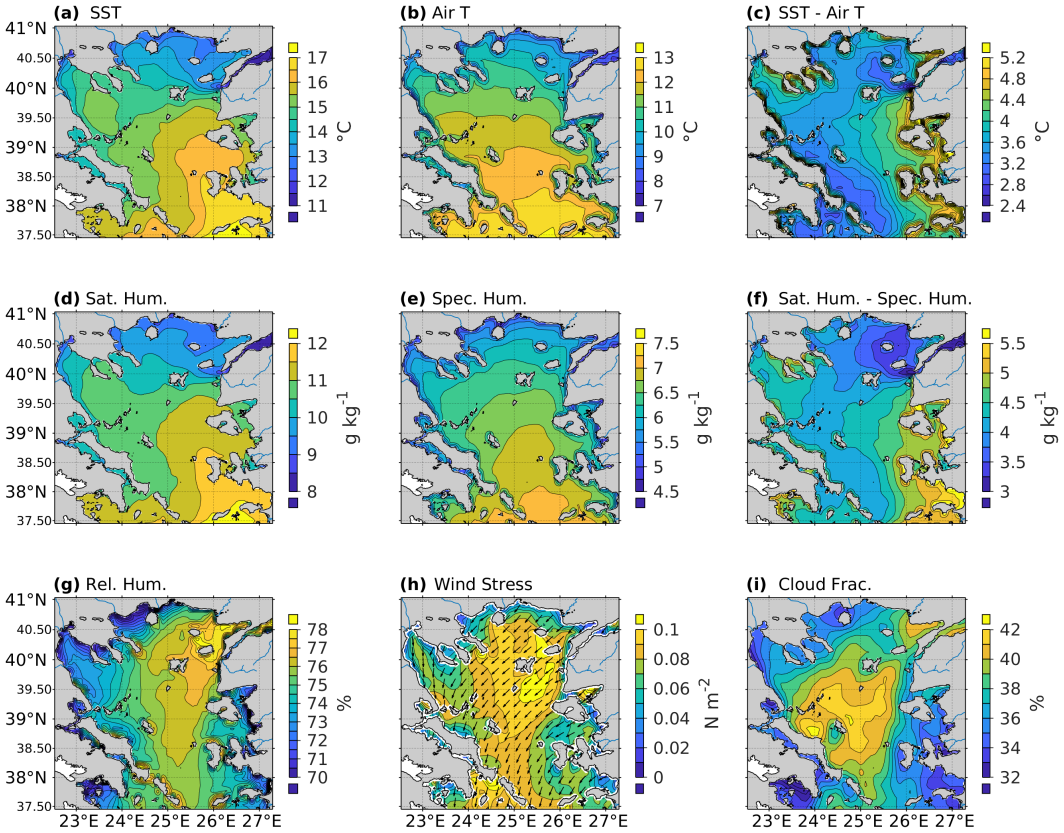

Figure S3: Spatial variability of parameters used for the calculation of thermal, freshwater and momentum surface fluxes from 2 December 2021 to 30 April 2022 over the study area. Time-mean (a) sea surface temperature (SST), (b) air temperature at 2 m height, (c) difference between SST and air temperature, (d) saturation humidity at sea surface, (e) specific humidity, (f) difference between saturation and specific humidity, (g) relative humidity, (h) wind stress magnitude and direction, and (i) cloud fraction.

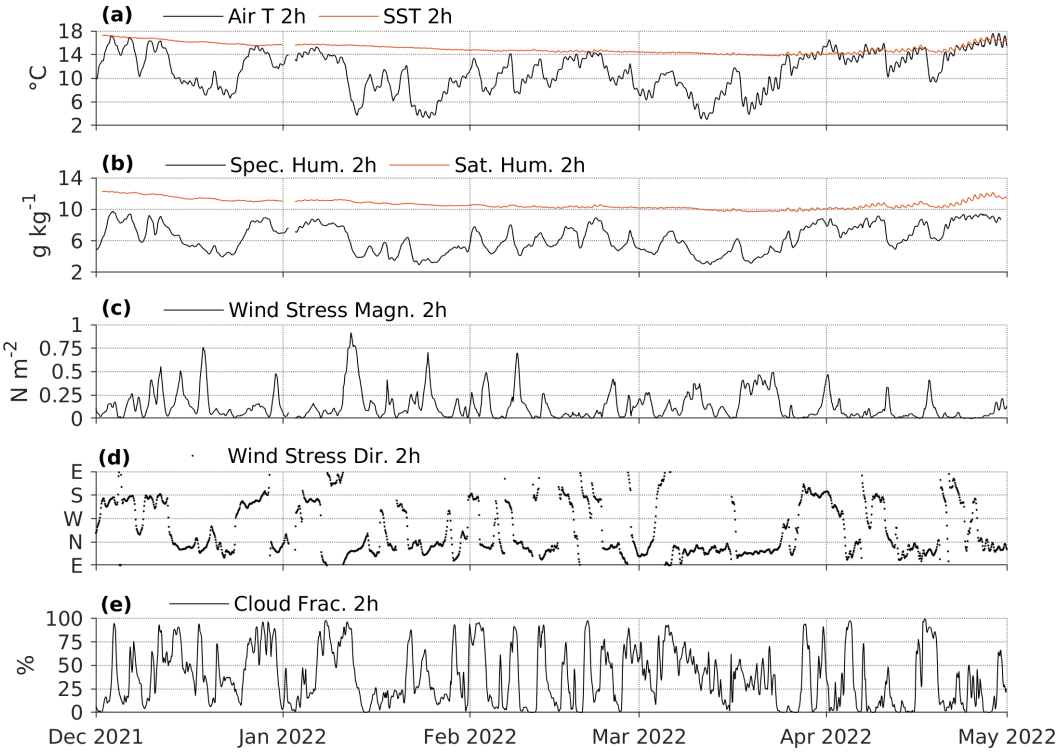

Figure S4: Temporal variability of parameters used for the calculation of thermal, freshwater and momentum surface fluxes from 2 December 2021 – 30 April 2022 over the study area. Field-mean (a) air temperature at 2 m height and sea surface temperature, (b) saturation humidity and specific humidity, (c) wind stress magnitude, (d) wind stress direction, and (e) cloud fraction.

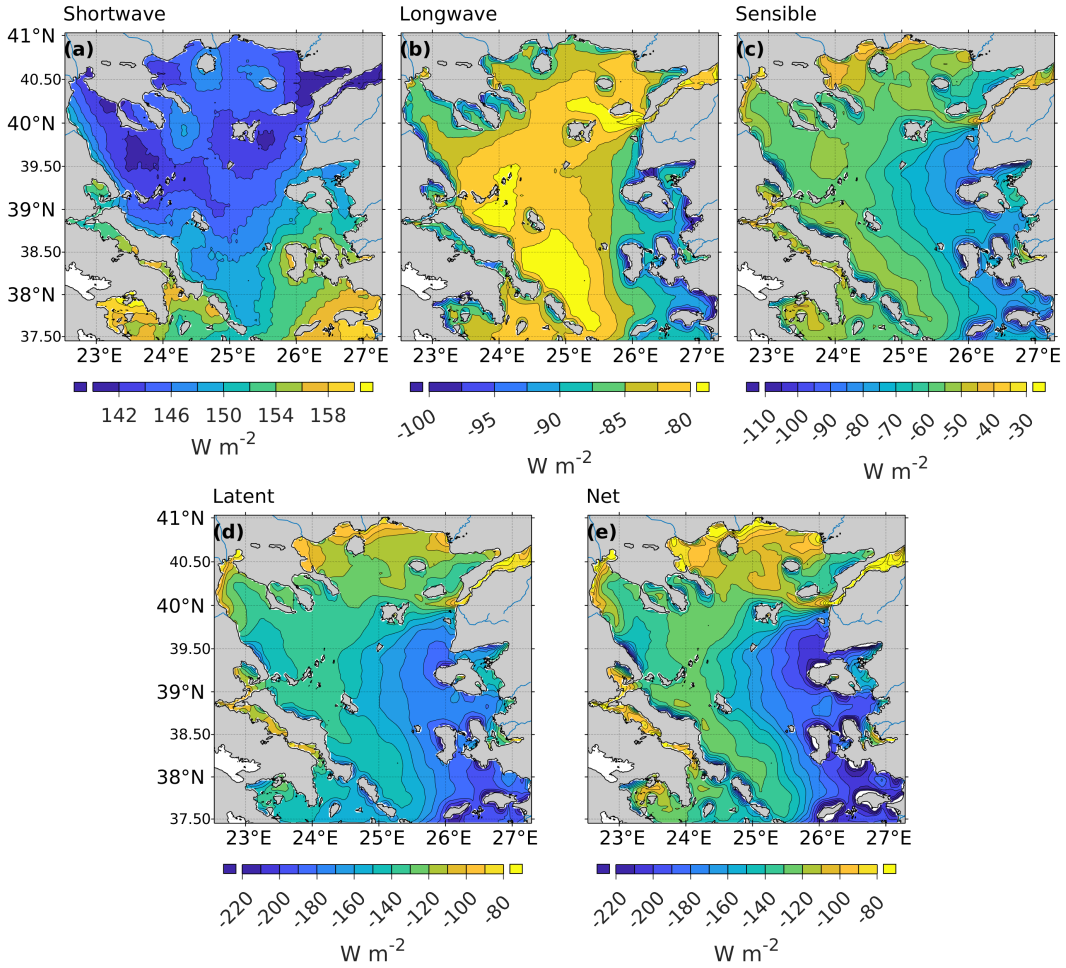

Figure S5: Time-mean surface heat flux components and net flux. (a) Shortwave, (b) net longwave, (c) sensible, (d) latent, and (e) net heat flux, averaged from 2 December 2021 to 30 April 2022.

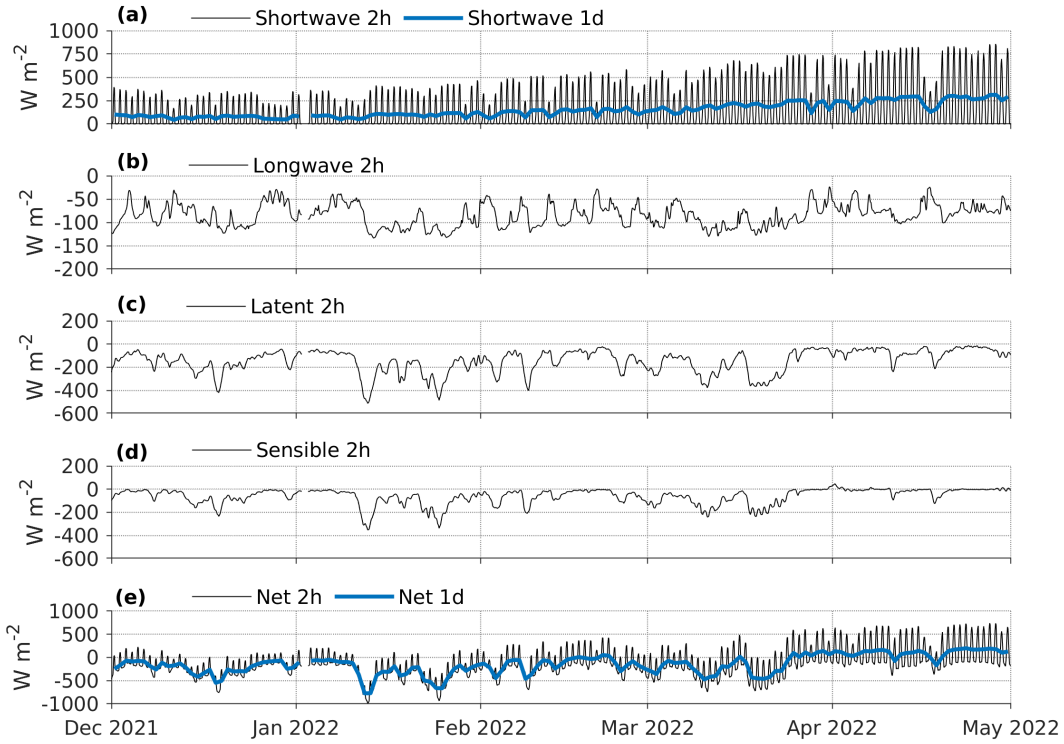

Figure S6: Field-mean surface heat flux components and net heat flux. (a) Shortwave, (b) longwave, (c) sensible, (d) latent, and (e) net heat flux, averaged over the North and Central Aegean Sea. Low-passed shortwave and net radiation is also shown.

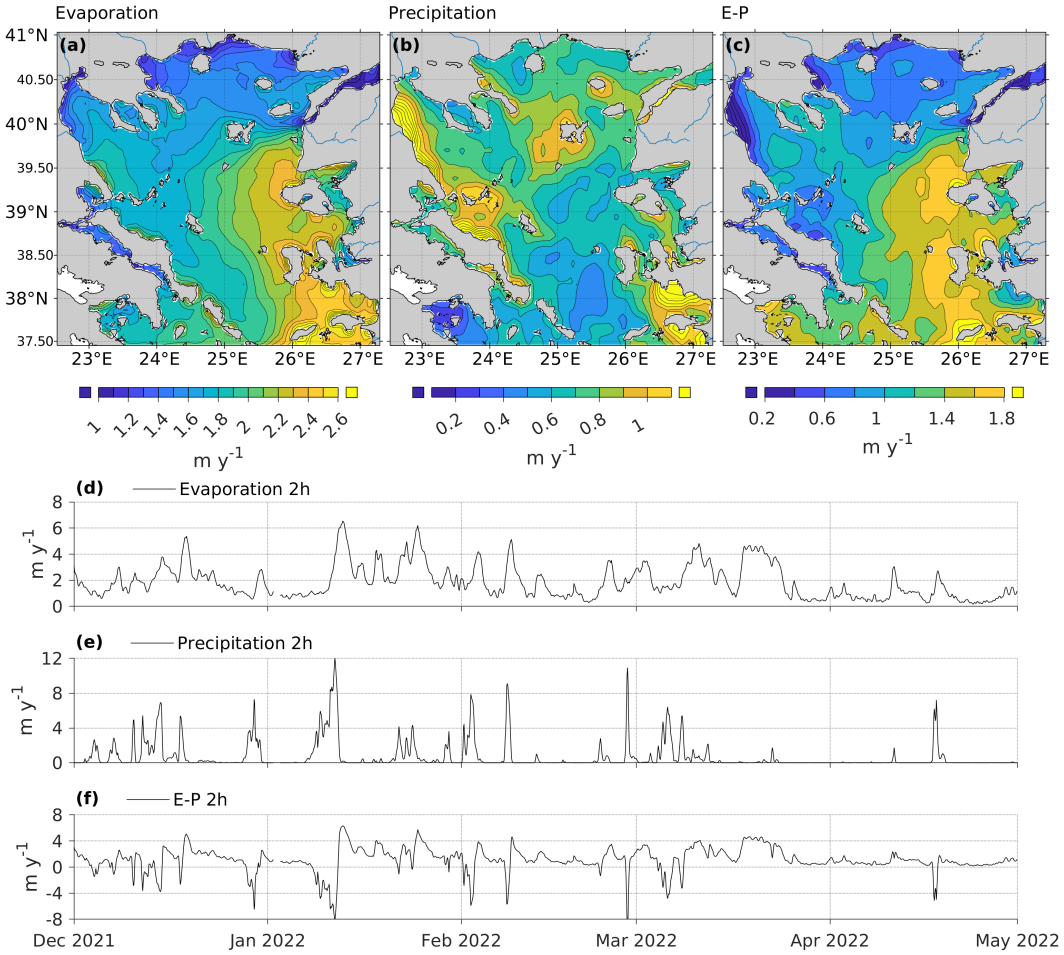

Figure S7: Time-mean and field-mean components of freshwater flux and net freshwater flux. Time-mean (a) evaporation, (b) precipitation, and (c) evaporation minus precipitation for the period 2 December 2021 – 30 April 2022. Field-mean (d) evaporation, (e) precipitation, and (f) evaporation minus precipitation, averaged over the North Aegean.

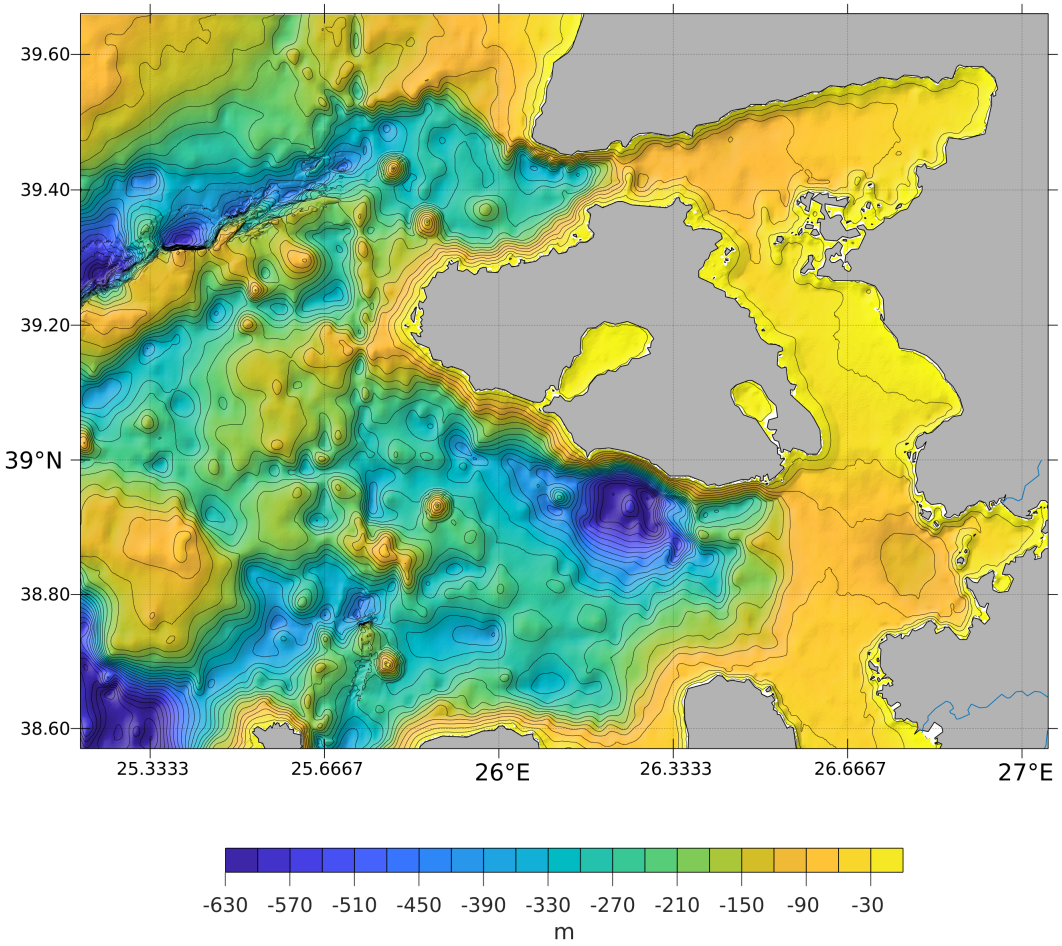

Figure S8: A close-up bathymetry map around Lesvos Island.

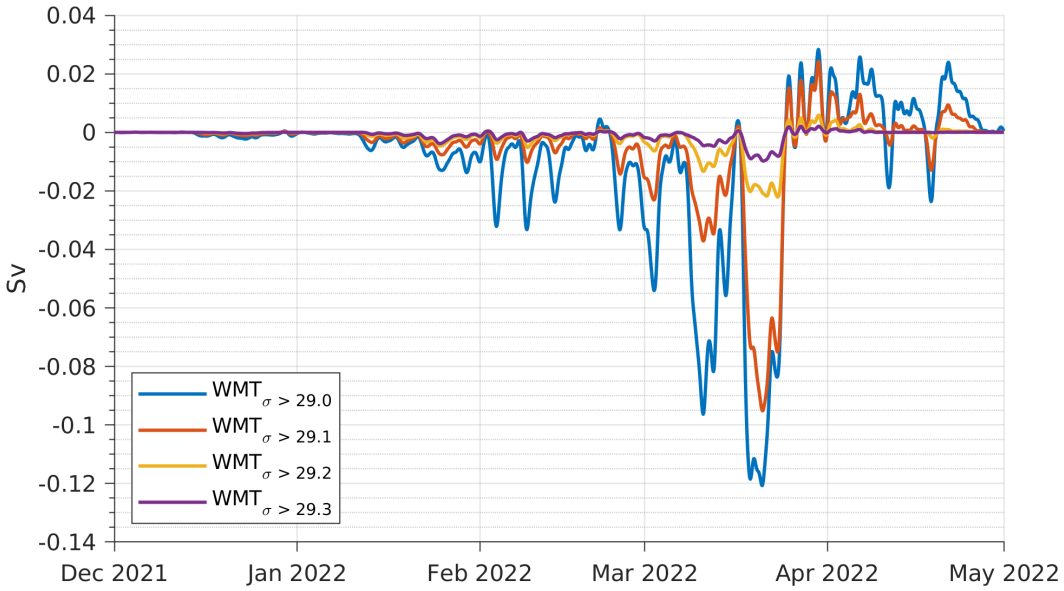

Figure S9: Atmospherically driven water mass transformation rates above the potential density thresholds 29, 29.1, 29.2, and 29.3 $\mathrm{kg\,m^{-3}}$.

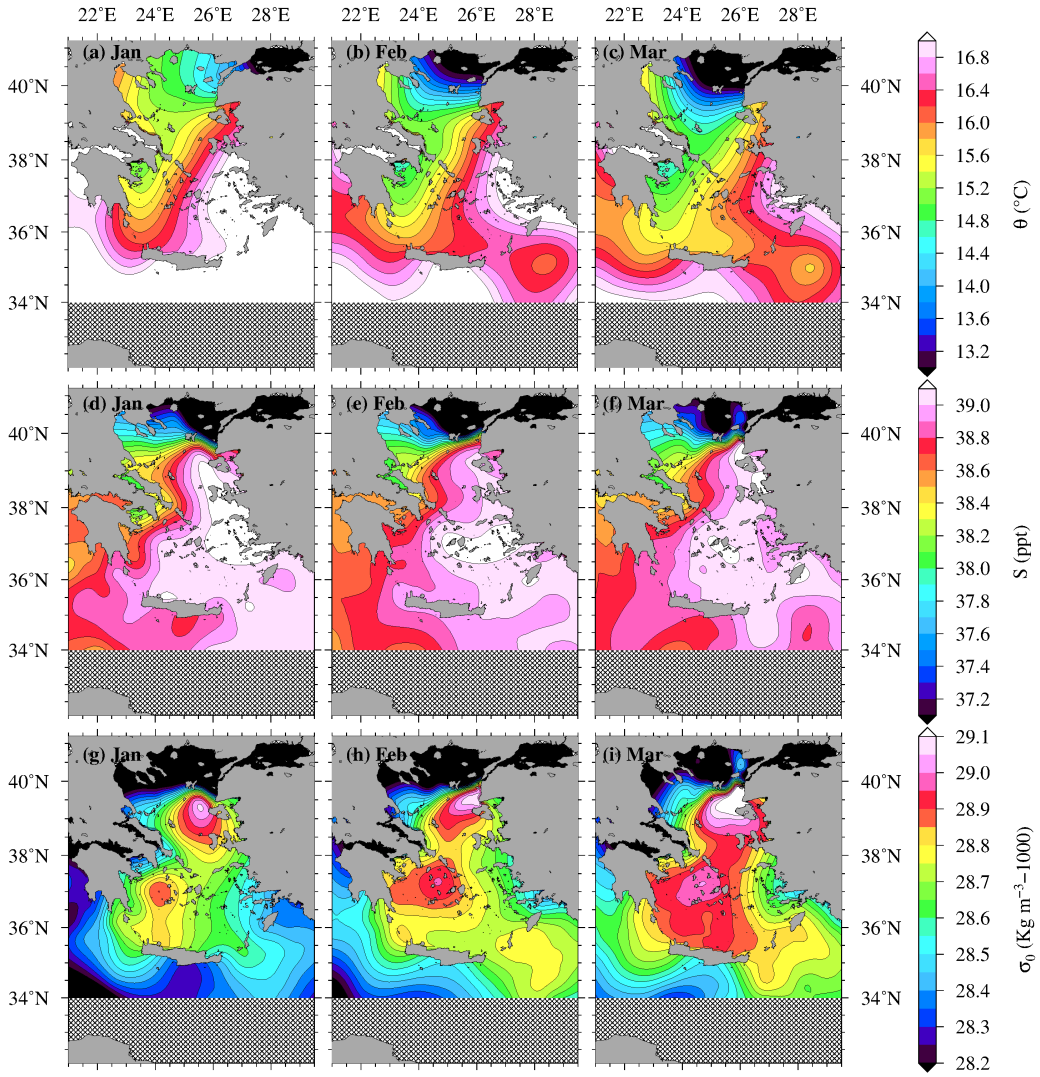

Figure S10: Winter climatology of (a, b, c) potential temperature, (d, e, f) salinity, and (g, h, i) potential density from MEDATLAS at 10 m depth.

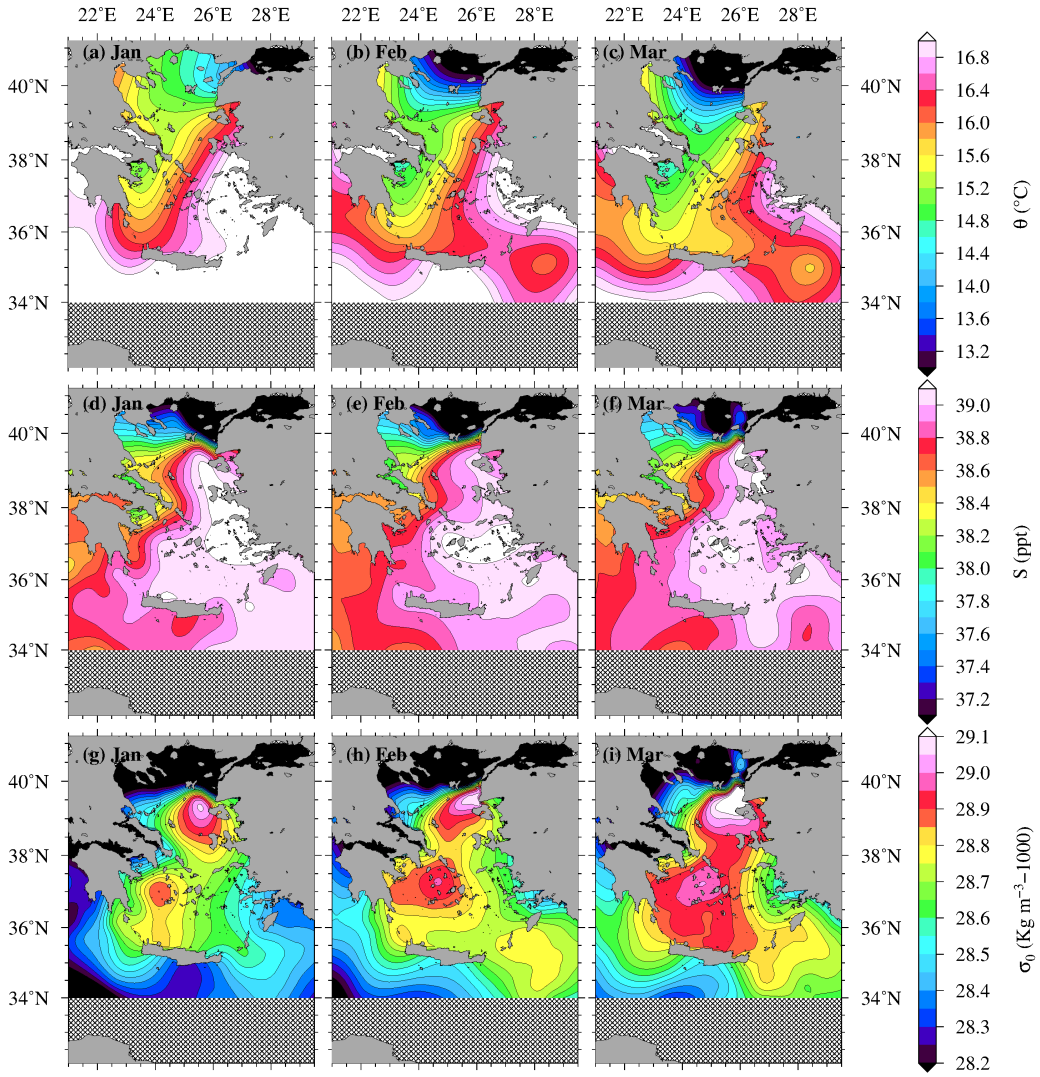

Figure S11: Winter climatology of (a, b, c) potential temperature, (d, e, f) salinity, and (g, h, i) potential density from Mediterranean Sea Hydrographic Atlas at 10 m depth.